Diffraction limited superresolution ptychography in the Rayleigh Sommerfeld regime

DANIEL CLAUS[1,2,*] AND JOHN MARIUS RODENBURG[2]

[1] *Institut für Lasertechnologien in der Medizin und Messtechnik, Universität Ulm, Helmholtzstrasse 12, 89081 Ulm, Germany*
[2] *Department of Electronic and Electrical Engineering, The University of Sheffield, Mappin Street, S1 3JD, UK*
[*] *Corresponding author: daniel.claus@ilm-ulm.de*

Superresolution in lensless near field ptychography is demonstrated via the application of a strongly curved illumination function. The reconstruction is performed using the Rayleigh-Sommerfeld diffraction integral, which is implemented via a pixel-size adjustable angular spectrum method. In this manner the reconstructed object details, which are not only smaller than the pixel-size of the sensor but even smaller than the smallest resolvable object detail defined by the effective NA of the 2D sensor, is enabled. The expected resolution, as predicted by the angles of scatter present in the optical configuration, is experimentally validated using a US air force resolution test target. The approach discussed here is not only limited to ptychography, but can be extended to other coherent diffractive imaging modalities such as object scanning holography or optical diffraction tomography, so as to enable high resolution near field quantitative phase imaging. © 2018 Optical Society of America

1. INTRODUCTION

Over the last decade ptychography has become one of the major methods of choice for coherent diffraction imaging. This is mainly due to the large amount of data diversity, which results in an extremely robust solution of the phase problem and can further be used to solve for the illumination function incident on the object [1–3], to perform superresolution imaging [4], to obtain three-dimensional properties of the object [5] and to correct experimental positioning errors [6–8]. It has therefore rapidly become an imaging method of choice in the synchrotron X-ray community [9], [10], electron microscopy [11], extreme ultraviolet light [12], and terahertz radiation [13], giving 2D images and tomographic reconstructions of materials and biological structures at unprecedented resolution and phase sensitivity.

It also has potentially wide applications in visible light imaging (even though very good focusing lenses are available), because the phase image it generates is quantitative, possesses a high contrast and is extremely sensitive, leading to applications in live cell imaging [14, 15] and surface metrology [16, 17].

Ptychography was originally postulated for applications where the detector is in the Fraunhofer region (which we will call 'Fraunhofer ptychography), as discussed in [18], but the technique can handle any object to detector propagator, as long as the form of that propagator is known. Near-field ptychography can be implemented in a projection configuration [19]. In this case, the illumination beam diverges from a source close to the specimen, resulting in a magnified image on the detector, which is of the form of a Gabor hologram with Fresnel fringes that encode the phase information. The relevant propagator is achieved computationally via the angular spectrum method [20]: the image on the detector is equivalent to that which would be obtained under plane wave illumination with the detector a short distance (relative to the validity of the Fresnel integral) downstream of the specimen. The magnification provided by the projection means that the physical pixel size can be much larger than the resolution element of the final reconstruction. For ptychography to work there has to be some structure in the illumination; in the divergent near-field configuration the incident wave must have significant phase perturbations so that as the object is moved, the recorded intensity varies, thus delivering the ptychographical diversity (there is no intensity variation if the illumination approximates to a plane wave). The divergent beam method holds the disadvantage that the amount of light entering the sensor is reduced (inverse square law), that it results in a smaller amount of transferred high spatial object frequencies [21], and that the reconstructed pixel-size depends on the divergence of the illumination function and hence cannot be changed once the image has been acquired. In [22] a near field ptychographic reconstruction technique, based on the angular

spectrum method, has been introduced, which is independent of the illumination function's curvature, while it offers an adjustment of the reconstructed pixel-size to any arbitrary value. It was demonstrated in [22] that it is possible to display object details smaller than the detectors pixel-size in accordance with the effective numerical aperture NA_{sensor} of the sensor, which is defined by the sensor-sample distance and the sensor size. Here, we would like to extent upon this work, demonstrating that the resolution in ptychography is not restricted by the effective NA of the sensor, but likewise depends on the numerical aperture of the illumination function NA_{Ill}. Hence, superresolved near field ptychographic reconstructions can be obtained.

It has been shown that in Fraunhofer ptychography it is possible to retrieve so-called 'superresolution' information [4]: in other words, it is able to recover the form of scattered radiation lying outside the effective numerical aperture of the detector. The extra information comes from rays in the illumination that are not parallel with the optic axis (similar to the convergent configuration, Fig. 1a). Even if these are destined to miss the detector entirely, they can be scattered from the object back into the detector. These scattering events have large scattering vectors (the difference between the incident and scattered wave vectors), corresponding to high resolution. Put in another way, the total information in the experiment comes from a convolution of incident ray angles and the angular size of the detector. This is identical to the resolution of a conventional microscope, with the extent of the convergent incident rays corresponding to the condenser lens aperture size and the detector size having the role of the object lens aperture. According to Abbe, the optical resolution is then defined by the NA_{sensor} and NA_{Ill}, the NA of the condenser [21]. Figure 1 shows by geometrical means how the total NA, resulting from the combination of the setup geometry and the curvature of the illumination employed can be calculated.

$$NA_{Comb} = \sin\left[\text{asin}(NA_{Ill}) + \text{asin}(NA_{Setup})\right] \\ \approx NA_{Ill} + NA_{Setup}. \tag{1}$$

The optical resolution limit can then be calculated as

$$P = \frac{\lambda}{NA_{Comb}}. \tag{2}$$

with P the smallest resolvable object period. However, compared to conventional microscopy, high resolution microscopic imaging is realised without any imaging lenses. Moreover, the high-resolution reconstruction extends over the entire field of view, whereas in conventional lens-based imaging it is usually confined to the region in close proximity to the optical axis only. In this paper we investigate a near-field ptychographical arrangement that uses convergent illumination and at the same time has the detector lying very close to the specimen, i.e. where we require the Rayleigh-Sommerfeld diffraction integral, implemented computationally by the angular spectrum method (Fig. 1a). Although the range of angles in the illumination and detector should define a high resolution in this configuration, one might suppose that this cannot be achieved in practice. We note that: (1) The angular spectrum propagation usually requires one-to-one correspondence between the exit wave pixel size of the object and the detector pixel size. We would therefore expect the detector pixel size to limit resolution. This, after all, is the rationale of the divergent beam method [19], which magnifies the Fresnel shadow image (Gabor hologram) to match pixel size with resolution, and the pixel-size adjustment algorithm

developed in [22]. (2) In fact, with convergent illumination, the shadow image is now demagnified, exacerbating (1). (3) At any one probe position, each part of the object is only subject to a localised area of the incident beam, which in turn has a very well-defined incident angle. Unlike Fraunhofer ptychography, now one diffraction pattern contains information scattered simultaneously from all parts of the illuminated area of the object and at all incident angles.

We show here that this is not the case. Resolution is in fact determined by a combination of the effective angular size of the detector (as subtended at the specimen) and the angular range of the incident radiation. In contrast to [19] the changed pixel size in the reconstruction process does not result from a divergent illumination function but can be controlled in the reconstruction process to any arbitrary value independent of the wavefront nature of the illumination function. This is accomplished via the addition of a numerical lens to the reconstruction process. A more detailed discussion of pixel-size adjustment via this numerical lens in combination with the angular spectrum method can be found in [22].

In this paper we theoretically and experimentally demonstrate for near field ptychography that a curved illumination function results in a superresolved reconstruction. This is based on a numerical aperture that exceeds the sensor's effective numerical aperture NA_{sensor},

$$NA_{Sensor} = \sin\left[\text{atan}\left(\frac{2d}{N\Delta x'}\right)\right] \approx \frac{2d}{N\Delta x'}, \tag{3}$$

with N the number of pixels and $\Delta x'$ is the size of a pixel-pitch, and where d is the object to detector distance. The illumination optics also has an angular range (See Fig. 1a).

The required parameters with respect to the necessary overlap between consecutive recording positions and the reconstruction method, based on an the angular spectrum method, are discussed in detail. Experimental results confirming the developed theory and demonstrating superresolved reconstruction will be shown.

In accordance with the categorization of diffraction limited superresolution optical systems provided by [23, 24] the superresolution algorithms discussed here, is based on increasing the space-bandwidth product via exploiting the temporal degree of freedom. In detail, multiple diffraction patterns hosting different spatial frequencies are sequentially recorded and combined to result in an increased frequency bandwidth and hence space-bandwidth product. The smallest resolvable periodic structure of the object P is defined by the effective NA_{Sensor} of the sensor is

$$P = \frac{\lambda d}{N\Delta x'}, \tag{4}$$

where λ is the wavelength, d is the recording distance, N number of pixels and $\Delta x'$ is the size of the pixel-pitch. In farfield ptychography [4] zero-padding is applied, which results in a smaller pixel-size in the reconstruction plane. This is due to the Fourier transform relationship between diffraction pattern and reconstruction plane. In that manner it becomes possible to display object details that are smaller than the sensor defined pixel-size in the reconstruction plane

$$\Delta x'' = \frac{\lambda d}{N\Delta x'} \tag{5}$$

with $\Delta x''$ the pixel-size in the reconstruction plane. In contrast to [4], the near field reconstruction method discussed here is

based on an adjusted angular spectrum method, as introduced in [22]. It has been implemented on the platform of the iterative ePIE algorithm [3], which we call Angular Spectrum ePIE and in its abbreviated form ASePIE. Advantages of the proposed technique compared to [4] are: i) reduction of the recording distance resulting in larger irradiance (inverse square law); reduced acquisition time , ii) a larger effective detector NA due to the reduced recording distance, iii) an increased correlation between measured modulus in diffraction space and in real space and hence a more representative error measure, and iv) increased stability and convergence compared to a far-field recording setup, as pointed out in [25].

2. METHODOLOGY

Launching higher diffraction angles into the sensor is achieved via moving the sample laterally across the curved illumination function, which can be considered as a combination of various plane wave components of different directionality. These higher diffraction angles correspond to high spatial frequencies. In order to enable the recording of the entire frequency bandwidth defined by the illumination function's numerical aperture, the object has to be moved across the illumination function with a certain degree of overlap between adjacent recording positions. This overlap is a function of the NA of the setup, which provides the acceptable frequency bandwidth within a single recording position, and the NA of the illumination function.

A measure of the required amount of overlap can be obtained from the ptychographic working principle, which is based on microinterference (overlap of diffraction orders) [18]. The interference pattern recorded represents a sinusoidal intensity pattern, which results in an ambiguous reconstruction with respect to the image and twin image. This is a well known problem in interferometry, which therefore requires the recording of further interferograms, which are characterized by an additional constant phase difference between object and reference wave. This phase difference is usually introduced via a piezo-mounted mirror in the reference arm [26].

In ptychography the ambiguity problem is solved via the application of a mutual lateral shift between object and illumination function, which results in a phase ramp across the entire diffraction pattern. In contrast to interferometry, not a constant phase is applied to the recorded intensity pattern, but a locally changing phase. This requires a different approach for investigating the recorded diffraction patterns, which is accomplished in an iterative manner. In [27] the ptychographic iterative engine (PIE) has been introduced and has been demonstrated in the visible regime and in the x-ray regime [28]. In [29] it has been demonstrated that a minimum amount of 60 percent overlap is required between consecutive recording positions using the PIE algorithm in order to successfully recover the complex excite wave. With the development of further ptychographic iterative algorithms, which enable the separation of illumination function and object function [1–3], the number of unknowns compared to the conventional PIE algorithms has consequently been increased, resulting in a larger amount of overlap.

Therefore, we introduce a factor f_s, representing how often the same object region has been sampled by the illumination function (with $f_s > 1/(1 - 0.6) = 2.5$ resulting from 60 percent overlap in PIE). Obviously in the periphery of the scan region the amount of sampling is reduced, hence resulting in a reduced resolution. Therefore, the following derivations refer to the maximum achievable resolution, which is applicable to scan areas exhibiting the same amount of maximum sampling.

$$\Delta\alpha = \alpha_1 - \alpha_2 = \frac{1}{f_s}\beta, \tag{6}$$

where $\Delta\alpha$ represents the change of tangential angle at the specimen between two consecutive recording positions and $\beta = \mathrm{asin}(NA_{Setup})$ is the semi recording angle defined by the setup geometry (specimen distance and detector size), as shown in Fig. 1(a) and (b). The angles α_1 and α_2 describe the angle between tangential plane wave component of the curved illumination function and the object plane.

In the following paragraph we would like to derive an expression, which relates the diffraction space condition, displayed in Eq. 6 into an object space condition with respect to the necessary lateral displacement or overlap between two consecutive recording positions. The spatial frequencies present in the object can be considered to be a composition of various sinusoidal frequency components. For a symmetrically positioned illumination function around the optical axis, the object region in close proximity to the optical axis experiences a plane wave component that is parallel to the orientation of the object and hence results in an α_1 of zero, see Fig. 1(a). A symmetrically distributed diffraction pattern is obtained on the sensor with zero (0_1), plus and minus first diffraction order (1_1 and -1_1, respectively), which result in the recording of low spatial object frequencies, represented by the low frequency sinusoidal squiggly line in Fig. 1(a). In this arrangement the maximum recordable spatial frequency is defined by the sensor's effective NA. If on the other hand the object is laterally displaced by an amount δ_x then the same object region experiences a plane wave component incident at a different angle α_2, which results in the recording of higher diffraction angles and hence higher spatial frequencies, represented by the high frequency sinusoidal squiggly line shown in Fig. 1(b). In that manner the resolution can be increased until the maximum diffraction angle defined by the combined NA of sensor and illumination function has been recorded. The probe is usually much smaller than the sensor. We can therefore assume that the semi recording angle β is the same in both recording positions. The recovery of the information provided by the entire NA_{Comb}, as defined in Eq. 1, requires more sampling positions, resulting in the following expression

$$\varnothing_{angle} \geqslant 1 - \frac{1}{f_s}\frac{\beta}{\beta + \alpha} = 1 - \frac{1}{f_s}\frac{\mathrm{asin}(NA_{Setup})}{\mathrm{asin}(NA_{Ill}) + \mathrm{asin}(NA_{Setup})} \tag{7}$$

with α representing the maximum tangential plane wave angle arising from the curved illumination function. The tangential difference angle $\Delta\alpha$ between two consecutive recording positions to ensure the necessary overlap is defined as

$$\Delta\alpha = \alpha\left(1 - \varnothing_{angle}\right). \tag{8}$$

Since ptychography is usually implemented using an x-y stage, the angular overlap $\varnothing_{angle}$ in the diffraction space needs to be translated into a lateral displacement δx and one-dimensional overlap $\varnothing_x$ in the object space. Due to the nonlinear sinusoidal relationship between angle and displacement, the minimum displacement arising at large illumination angles is taken into account. With the help of trigonometric relationships derived from Fig. 1(c), the corresponding lateral displacement can be calculated as:

$$\delta x = \frac{D}{\tan\alpha}\tan\left(\frac{\Delta\alpha}{2}\right) \approx \frac{D}{2}\left(1 - \varnothing_{angle}\right). \tag{9}$$

Consequently the lateral one dimensional overlap $\varnothing_x$ becomes

$$\varnothing_x = \frac{D - \delta x}{D} \approx \frac{1}{2}\left(1 + \varnothing_{angle}\right). \tag{10}$$

The parameters derived above, provide a measure at which the entire spatial frequencies bandwidth of the optical system is well sampled and can be retrieved in the reconstruction process. The iterative reconstruction process is in analogy with ePIE [3] performed in sequential order. A single iteration consists of propagating the product of starting guesses for object function and illumination function to the diffraction plane, where the modulus is replaced by the square root of the recorded diffraction pattern's intensity. Afterwards, an inverse propagation to the object plane is performed for each updated complex diffraction pattern. In a next step the updated excite wave, becomes separated using two update functions, one for the object function and one for the illumination function. Taking into account the stage positions used in the recording process enables the correct lateral assembly of the updated object function, which represents the end of one iteration. In our case the relationship between object space and diffraction space is not based on a farfield relationship, Fraunhofer- or Fresnel approximation, implemented via the Fourier transformation, but on the near field relationship, scalar Rayleigh-Sommerfeld diffraction integral, implemented via the angular spectrum method combined with spherical numerical lens, see [22] for more detailed discussion. The focal length of the numerical lens is defined as:

$$f = \frac{d \cdot \beta'}{1 - \beta'}; \tag{11}$$

whereas the magnification β' is defined as the ratio between original sensor pixel-size and the desired pixel-size in the object space. Hence, to display object details smaller than the sensor's pixel-size a β' large than 1 has to be chosen. The spatial frequency response from a scanned finite region of the specimen have been recorded in different diffraction patterns. Via the updating process and the choice of a corresponding β' in the reconstruction process, the information from the different diffraction patterns becomes reassembled to result in a full spatial frequency range reconstruction. In order to ensure unaliased representation of high spatial frequencies the smallest resolvable object periodicity should be displayed by more than two pixels. We have chosen four pixels, which represents a good match between recorded and available frequency bandwidth defined by the number of pixels. A larger ratio is not recommended since it results in empty magnification without adding information content. Hence, the numerical magnification that has to be applied to ASePIE is:

$$\beta' = \frac{4\Delta x'}{P} = \frac{4\Delta x'\left(NA_{ill} + NA_{Setup}\right)}{\lambda}, \tag{12}$$

where $\Delta x'$ is the size of the detector's pixel pitch and P is the smallest resolvable object period (twice the size of the smallest resolvable object detail), see Eq. 2.

3. EXPERIMENT

A HeNe-laser (λ=632.8nm) has been used for the experiment. The laser light has been launched into a single mode fibre (Thorlabs SM450) with an NA of roughly 0.14. A convex lens of 15 mm focal length (Thorlabs LA1540-A) has been employed to converge the light towards the sample. The lens was positioned

at a distance of 36 mm to excite of the fibre. The sample was positioned at 22 mm distance downstream from the lens. A square aperture of 1.6 mm edge length with a latent milled square of 100 microns length in both dimensions, as reported in [31] was mounted at a distance of 6 mm upstream in front of the sample. The square aperture with the latent point at one of the corners holds the advantage that it breaks the symmetry and hences introduces a larger degree of diversity in the probe compared to a circular probe, as reported in [30]. The sample was positioned at a distance of approximately 1 mm in front of the focal plane. The diffraction patterns have been recorded in a lensless manner, as schematically shown in Fig. 2. A CCD camera has been employed with 2048x2048 pixels and 7.4 μm pixel pitch. For demonstration purposes only 512x512 pixels have been used, which with a sample-sensor distance of 15 mm results in a NA_{Setup} of 0.125. The NA of the illumination function can approximately be obtained from the experimental arrangement e.g. distance fibre to lens, focal length of lens, distance lens to object. On the other hand, the ASePIE algorithm already delivers a more accurate estimate due to the recovery of the complex illumination function. The illumination function's corresponding NA_{ill} can be then be obtained via propagation to different planes using the angular spectrum method. At each propagation distance the central section is cropped in x and y, which when stitched result in a longitudinal propagation profile for both lateral dimensions, as shown in Fig. 3. The semi illumination angle obtained is 7.2°, which corresponds to an NA_{ill} of 0.125, resulting in a combined NA_{Comb} of 0.25 and a theoretical resolution of 2.5 μm period. The size of the illumination function at the sample plane is 240 μm in for both sides, as shown in Fig. 3 (a) and (b) for amplitude and phase, respectively. Due to diffraction on the edge of the square aperture the illumination function shows some ringing artifacts at the edges.

In order to establish the necessary amount of object-sampling factor f_s, experiments with different amount of overlap have been conducted. In each experiment a grid of 10x10 positions has been employed. Starting from 60% the amount of overlap was changed in 5% steps to 95% overlap. In Fig. 4(a-d), the results obtained for 70 %, 80%, 90% and 95% overlap are shown. In accordance with Eq. 12, a magnification of 10 was employed in the ASePIE algorithm to make sure that the smallest resolvable object detail can be displayed. 600 Iterations have been used to obtain a good reconstruction. It was realised that the best reconstructions could be obtained with a lateral overlap $\varnothing_x$ of 95 % (resulting in δx=12 μm, and an angular overlap $\varnothing_{angle}$=90 %). This corresponds to a sampling factor of five (rearranging Eq. 7 to solve for f_s). The sampling factor obtained matches well with the existing literature for separate recovery of object and illumination function [19]. A theoretical explanation is provided by doubling the amount of unknowns from PIE to ePIE, represented by the sum of complex valued object function and illumination function.

In order to determine the resolution achieved an objective measure has been generated. All cross sections across the test-target element under investigation have been averaged enabling a representative measure with respect to the contrast across the entire test target element. Care was taken that the three local minima (black strips) are visible and the ratio of the largest local minima to the smallest local maxima is less than 0.81 according to Rayleigh's resolution criterion for a rectangular aperture, as discussed in [32]. In horizontal direction group 8 element 4 (period of 2.76 μm) and in vertical direction group 8 element 6 (period of 2.2 μm) could be resolved with an intensity ratio of 0.28 and

0.4 respectively. This demonstrates that a good match between theoretical prediction and experimental result could be obtained. In order to highlight the increase in resolution the same diffraction patterns have been used in a conventional ePIE reconstruction using the same amount of iterations. At first the same diffraction pattern region of 512x512 pixels (same effective NA_{setup} of the detector 0.125), and secondly a region of 1024 x 1024 pixels (effective NA_{setup} of detector equals 0.25), have been investigated. The corresponding ePIE reconstructions are shown in Fig. 5(b) for 512 x 512 pixels (horizontal and vertical group 7 element 5; period of 4.92 μm) and Fig. 5(c) for 1024 x 1024 pixels (horizontal group 8 element 1 and vertical group 8 element 4; periods of 3.9 μm and 2.76 μm, respectively). Hence, the resolution obtained with ePIE is in both cases lower than when employing ASePIE method. In particular for the 1024 x 1024 pixels ePIE reconstruction a larger resolution (theoretical period of 2.5 μm) would have been anticipated. The reduced resolution is likely to be due to the large effective sensor NA, which requires the application of the angular spectrum method instead of the paraxial approximation used in the conventional ePIE algorithm. The error measure for ASePIE at 512 x 512 pixels, ePIE at 512x512 pixels and ePIE at 1024x1024 pixels are shown in Fig. 6. It can be noticed that ePIE converges quicker with respect to the gradient of the error curve. This effect is mainly due to the smaller reconstructed pixel size in ASePIE, which necessitates extracting the high frequency information. The high frequency information is represented in the diffraction patterns as low intensity counts, which in the recorded diffraction patterns is located distant from the bright field disc in close proximity of the optical axis. Extracting the high frequency information hence requires multiple iterations. Another low count intensity region is represented by the diffraction patterns, which have been recorded at the edge of the scanned area. In this case these areas have been sampled less often than the inside areas and are hence represented with reduced contrast. In comparison to ePIE, ASePIE does not manage to reconstruct these object regions with high contrast. A possible explanation is that ASePIE needs to extract more information from the diffraction patterns using the same amount of iterations.

4. CONCLUSION

The ptychographic resolution enhancement capability first demonstrated in [4] could be extended within the Rayleigh-Sommerfeld regime. A theoretical account of the combined resolution of the illumination function's NA_{ill} and effective setup NA_{setup}, the required overlap to enable sufficient sampling of the high resolution information and the required numerical magnification to enable displaying the smallest resolvable object detail has been presented. Those theoretical values have experimentally been validated and in our case the resolution, as defined by the NA_{setup} of the setup, could be more than doubled (2.2 μm compared to 5 μm). Numerous advantages of the discussed method exist, among others: better usage of the sensors space bandwidth product, more compact setup and increased stability and convergence. It will therefore be very useful not only for visible light applications, but also for other regions of the electromagnetic spectrum, where the phase signal represents an important source of information/contrast mechanism e.g. coherent X-ray imaging.

(a)

(b)

(c)
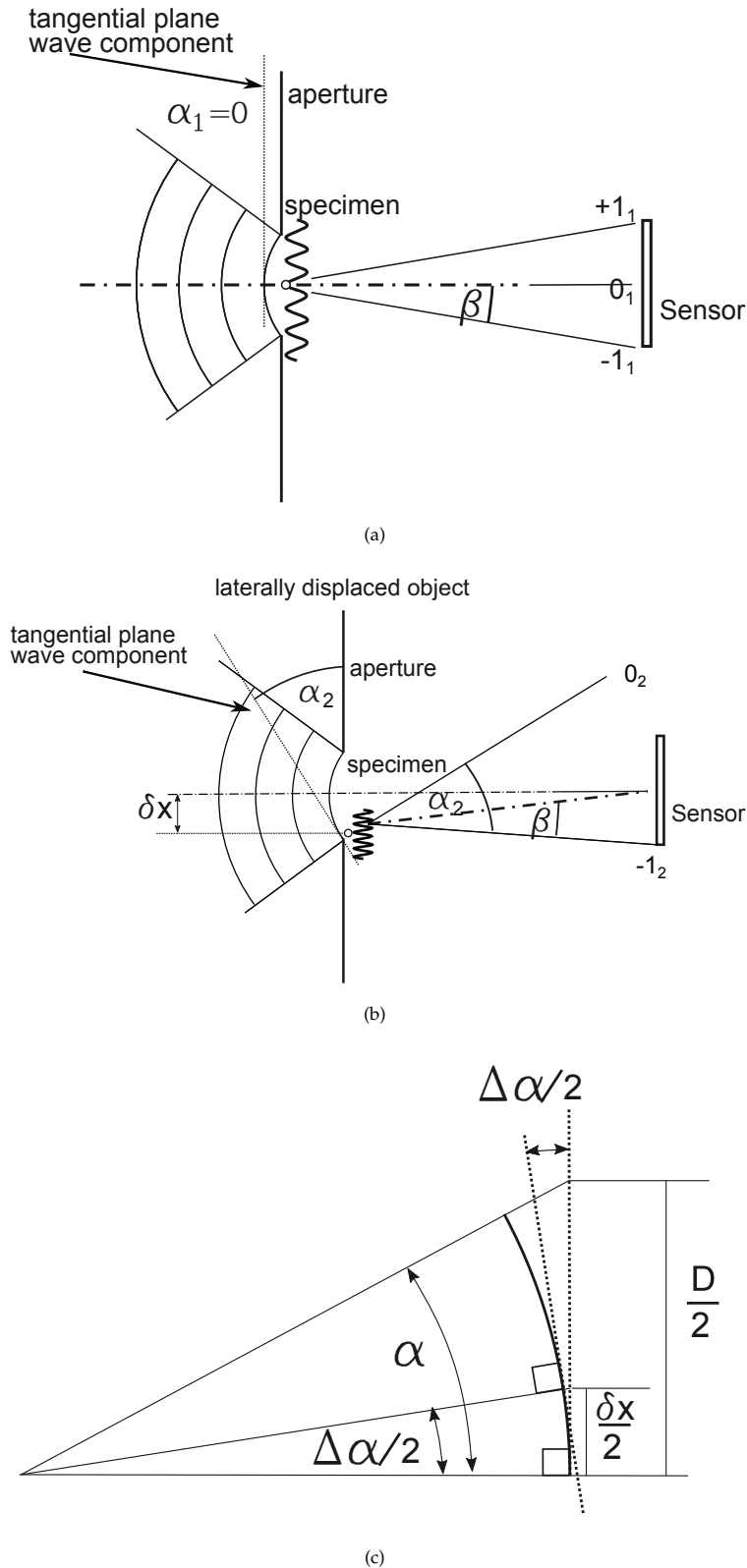
Fig. 1. (a) Centre of illumination function and centre of aperture coincide , (b) displacement δx results in de-centered illumination function and the recording of higher diffraction angles, (c) smallest lateral shift δx in order to sample the object's high spatial frequencies arising from the illumination function of semi angle α with the angular overlap $\varnothing_{angle}$ (half angle $\Delta\alpha$ and corresponding lateral shift δx account for possible opposite direction of incident plane wave component, which results in doubling the angular range to 2α, as to record plus and minus first maximum diffraction order)
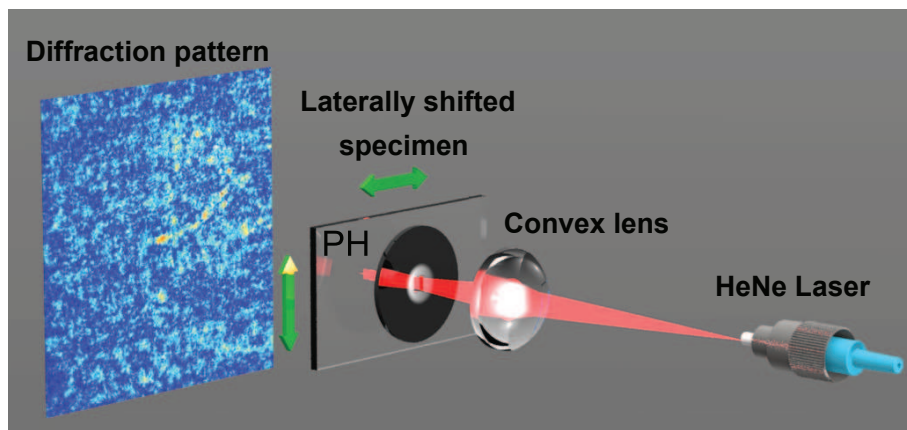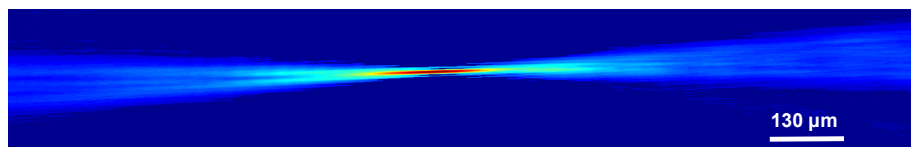
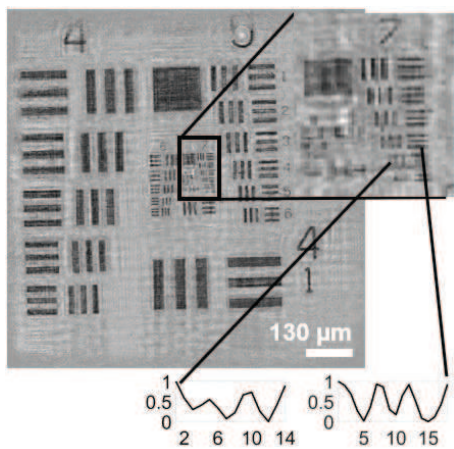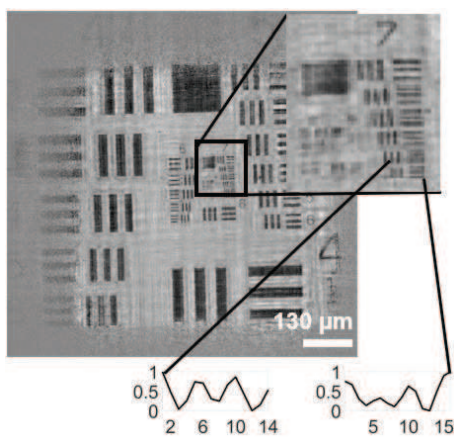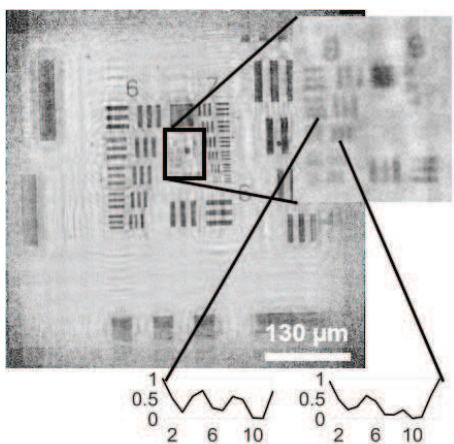**Fig. 2.** Schematic sketch of setup geometry
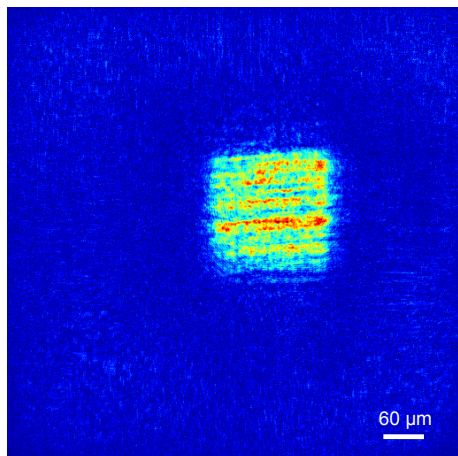
(a)
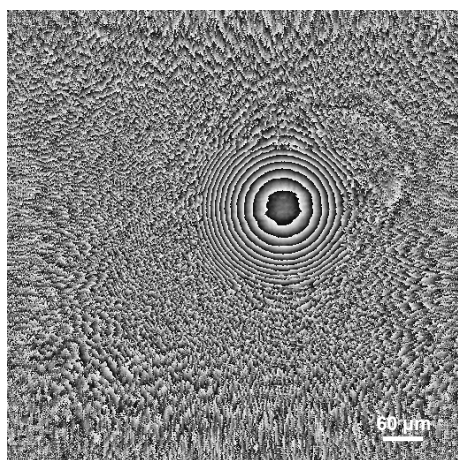
(b)
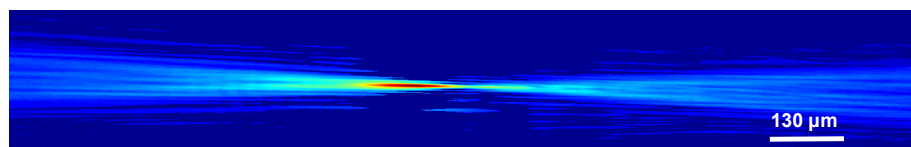
(c)

(d)

Fig. 3. Illumination function (a) intensity, (b) phase, (c) Intensity of axial beamprofile in vertical direction, (d) intensity of axial beamprofile in horizontal direction
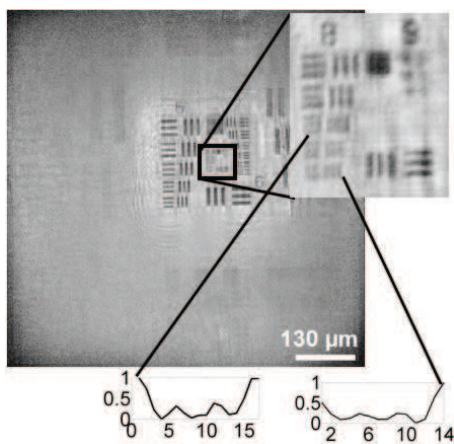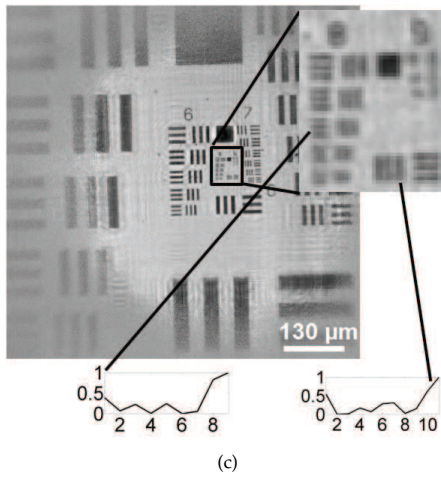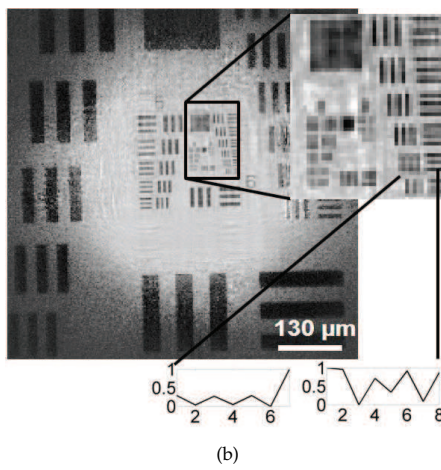
(a)
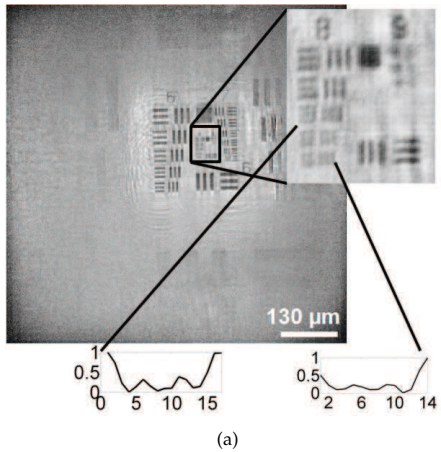
(b)

(c)

(d)

Fig. 5. (a) Angular Spectrum ePIE intensity reconstruction for ten times magnification (512 x 512 cropped diffraction patterns), (b) ePIE intensity reconstruction obtained from 512 x 512 pixels cropped diffraction pattern, (c) ePIE intensity reconstruction obtained from 1024 x 1024 pixels pixels cropped diffraction patterns
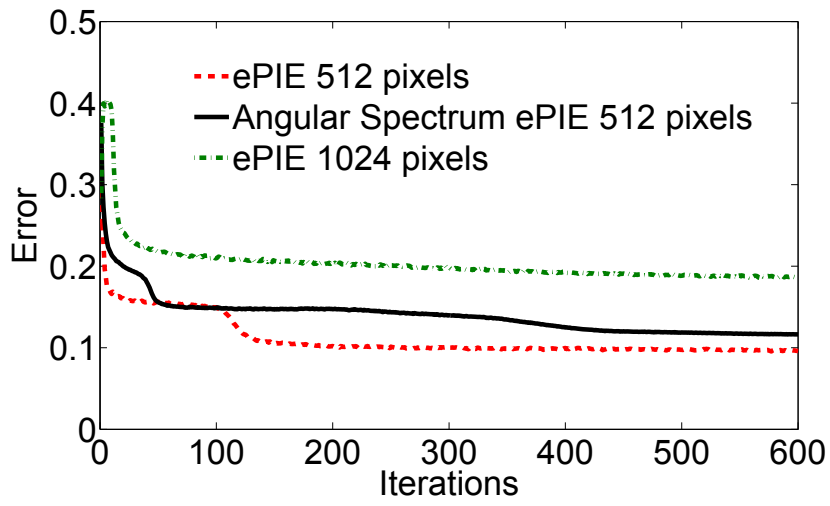
Fig. 6. Error metric for ePIE at 512x512 pixels, ASePIE at
512x512 pixels, and ePIE at 1024x1024 pixels

REFERENCES

1. O. Thibault, M. Dierolf, A. Menzel, O. Bunk, C. David, and F. Pfeiffer, "High-resolution scanning x-ray diffraction microscopy," Science **321**, 379–382 (2008).
2. P. Thibault, M. Dierolf, O. Bunk, A. Menzel, and F. Pfeiffer, "Probe retrieval in ptychographic coherent diffractive imaging," ultramicroscopy **109**, 338–343 (2009).
3. A. M. Maiden and J. M. Rodenburg, "An improved ptychographical phase retrieval algorithm for diffractive imaging," Ultramicroscopy **109**, 1256–1262 (2009).
4. A. M. Maiden, M. J. Humphry, F. Zhang, and J. M. Rodenburg, "Super-resolution imaging via ptychography," J. Opt. Soc. Am. A **28**, 604–612 (2011).
5. A. M. Maiden, M. J. Humphry, and J. M. Rodenburg, "Ptychographic transmission microscopy in three dimensions using a multi-slice approach," J. Opt. Soc. Am. A **29**, 1606–1614 (2012).
6. M. Guizar-Sicairos and J. R. Fienup, "Phase retrieval with transverse translation diversity: a nonlinear optimization approach," Opt. Express **16**, 7264–7278 (2008).
7. A. M. Maiden, M. J. Humphry, M. C. Sarahan, B. Kraus, and J. M. Rodenburg, "An annealing algorithm to correct positioning errors in ptychography." ultramicroscopy **120**, 64–72 (2012).
8. F. Zhang, I. Peterson, J. Vila-Comamala, A. Diaz, F. Berenguer, R. Bean, B. Chen, A. Menzel, I. K. Robinson, J. M. Rodenburg "Translation position determination in ptychographic coherent diffraction imaging ." Opt. Express **21**, 13592–13606 (2013).
9. M. J. Holler, A. Diaz, M. Guizar-Sicairos, P. Karven, E. Farm, E. Harkonen, M. Ritala, A. M. J. Raabe, and O. Bunk, "X-ray ptychographic computed tomography at 16 nm isotropic 3d resolution," Scientific Reports **4**, 3857 (2014).
10. M. J. Holler, M. Guizar-Sicairos, E. H. R. Tsai, R. Dinapoli, E. Muller, O. Bunk, J. Raabe, and G. Aeppli, "High-resolution non-destructive three-dimensional imaging of integrated circuits," Nature **543**, 7645 (2017).
11. Y. Jiang, Z. Chen, Y. Han, P. Deb, H. Gao, S. Xie, Y. Purohit, M. W. Tate, J. Park, S. M. Gruner, V. Elser, D. A. Muller "Electron ptychography of 2D materials to deep sub-ångström resolution," Nature **559**, 343–349 (2018).
12. D. F. Gardner, M. Tanksalvala, E. R. Shanblatt, X. Zhang, B. R. Galloway, C. L. Porter, R. Karl Jr, C. Bevis, D. E. Adams, H. C. Kapteyn, M. M. Murnane, G. F. Mancini, "Subwavelength coherent imaging of periodic samples using a 13.5 nm tabletop high-harmonic light source," Nature Photonics **11**, 259–263 (2017).
13. L. Valzania, T. Feurer, P. Zolliker, and E. Hack , "Terahertz ptychography," Opt. Lett. **43**, 3, 543–546 (2018).
14. J. Marrison, L. Räty, P. Marriott, and P. O'Toole, "Stain-free imaging of a549 cells using quantitative phase information," in "EMC Conference, Birmingham, UK 2011," (2011).
15. D. Claus, A. M. Maiden, F. Zhang, F. G. R. Sweeney, M. J. Humphry, H. Schluesener, and J. M. Rodenburg, "Quantitative phase contrast optimised cancerous cell differentiation via ptychography," Opt. Express **20**, 9911–9918 (2012).
16. A. M. Maiden, J. M. Rodenburg, and M. J. Humphry, "Optical ptychography: a practical implementation with useful resolution," Opt. Lett. **35**, 2585–2587 (2010).
17. D. Claus, D. J. Robinson, D. G. Chetwynd, Y. Shuo, W. T. Pike, J. J. D. J. T. Garcia, and J. M. Rodenburg, "Dual wavelength optical metrology using ptychography," J. Opt. **15**, 035702 (2013).
18. J. Rodenburg, "Ptychography and related diffractive imaging methods," Advances in Imaging and Electron Physics **150**, 87–184 (2008).
19. M. Stockmar, P. Cloetens, I. Zanette, B. Enders, M. Dierolf, F. Pfeiffer, and P. Thibault, "Near-field ptychography: phase retrieval for inline holography using a structured illumination," Scientific Reports **3**, 1927 (2013).
20. J. W. Goodman, *Introduction to Fourier Optics* (McGraw-Hill, San Francisco, 1968), 1st ed.
21. E. Abbe, "Beitrag zur theorie des mikroskops und der mikroskopischen auflösung," Archiv für mikroskopische Anatomie **9**, 413–468 (1873).
22. D. Claus and J. M. Rodenburg, "Pixel size adjustment in coherent diffractive imaging within the rayleigh–sommerfeld regime," Appl. Opt. **54**, 1936–1944 (2015).
23. W. Lukosz, "Optical systems with resolving powers exceeding the classical limit," J Opt Soc Am **56**, 1463–1472 (1966).
24. W. Lukosz, "Optical systems with resolving powers exceeding the classical limit. ii," J Opt Soc Am **57**, 932–941 (1967).
25. G. J. Williams, H. M. Quiney, A. G. Peele, and K. A. Nugent, "Fresnel coherent diffractive imaging: treatment and analysis of data," New J. Phys. **12**, 035020 (2010).
26. J. C. Wyant, "lecturenotes: Modern optical testing," (2009).
27. J. M. Rodenburg and H. M. L. Faulkner, "A phase retrieval algorithm for shifting illumination," Appl.Phys.Lett. **85**, 4795–4797 (2004).
28. J. M. Rodenburg, A. C. Hurst, and A. G. Cullis, "Transmission microscopy without lenses for objects of unlimited size," Ultramicroscopy **107**, 227–231 (2007).
29. O.Bunk, M. Dierolf, S. Kynde, I. Johnson, O. Marti, and F. Pfeiffer, "Influence of the overlap parameter on the convergence of the ptychographic iterative engine," ultramicroscopy **108**, 481–487 (2008).
30. J. R. Fienup, "econstruction of object having a latent reference point," J. Opt. Soc. Am. **73**, 1421–1426 (1983).
31. D. J. Batey, D. Claus, J. M. Rodenburg, "Information multiplexing in ptychography.," ultramicroscopy **138**, 13–21 (2014).
32. D.Claus and D. Iliescu, "Optical parameters and space–bandwidth product optimization in digital holographic microscopy," Appl. Opt. **52**, 410–422 (2012).